



High-Order FDTD Schemes for Maxwell's Interface Problems with Discontinuous Coefficients and Complex Interfaces Based on the Correction Function Method

Yann-Meing Law¹ · Jean-Christophe Nave¹

Received: 29 July 2021 / Revised: 22 January 2022 / Accepted: 5 February 2022 /
Published online: 8 March 2022

© The Author(s), under exclusive licence to Springer Science+Business Media, LLC, part of Springer Nature 2022

Abstract

We propose high-order FDTD schemes based on the Correction Function Method (CFM) (Marques et al. in *J Comput Phys* 230:7567–7597, 2011) for Maxwell's interface problems with discontinuous coefficients and complex interfaces. The key idea of the CFM is to model the correction function near an interface to retain the order of a finite difference approximation. To do so, we solve a system of PDEs based on the original problem by minimizing an energy functional. The CFM is applied to the standard Yee scheme and a fourth-order FDTD scheme. The proposed CFM-FDTD schemes are verified in 2-D using the transverse magnetic (TM_z) mode. Numerical examples include scattering of magnetic and non-magnetic dielectrics, and problems with manufactured solutions using various complex interfaces and discontinuous piecewise varying coefficients. Long-time simulations are also performed to investigate the stability of CFM-FDTD schemes. The proposed CFM-FDTD schemes achieve up to fourth-order convergence in L^2 -norm and provide approximations devoid of spurious oscillations.

Keywords Interface conditions · Maxwell's equations · Correction function method · Finite-difference time-domain · High order

Mathematics Subject Classification 35Q61 · 65M06 · 78M20 · 78A45

1 Introduction

In computational electromagnetics, the development of finite difference (FD) strategies to tackle Maxwell's interface problems remains a challenge [27]. Indeed, one should expect from a numerical approach to treat arbitrary complex geometries of the interface without

✉ Yann-Meing Law
yann-meing.law-kamcio@mail.mcgill.ca

Jean-Christophe Nave
jean-christophe.nave@mcgill.ca

¹ Department of Mathematics and Statistics, McGill University, Montréal, QC H3A 0B9, Canada

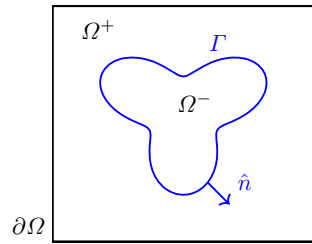
increasing the complexity of the method, achieve high-order convergence to diminish the phase error for long-time simulations [12], and handle discontinuous coefficients and discontinuous solutions, to name a few. The potential lack of regularity of the solution of such problems is a well-known challenge [10, 16, 18]. Moreover, FD schemes often use simple Cartesian mesh grids, and therefore the representation of the interface and the enforcement of interface conditions, fundamental to obtain accurate results, are far from trivial. Hence, a first approach that consists of a staircased approximation of the interface and the use of the well-known Yee scheme [25], which is a second-order finite-difference time-domain (FDTD) scheme, yields a first-order scheme at best and non-convergent approximations in some cases [8].

Several numerical strategies have been proposed to overcome these issues. A staircase-free second-order FDTD scheme, which explicitly enforces interface conditions, is proposed in [8]. This numerical strategy has been verified for non-magnetic dielectric and perfect electric conductor (PEC) problems using a 2-D transverse magnetic (TM) form of Maxwell's equations [8, 9]. Inspired by the Immersed Interface Method (IIM) [16], an Upwinding Embedded Boundary (UEB) method has also been developed to obtain a global second-order scheme to treat magnetic and non-magnetic dielectric problems using a TM form of Maxwell's equations [5]. In the same vein, high-order FDTD schemes based on the Matched Interface and Boundary (MIB) method have been proposed in [28]. These strategies derive and use jump conditions to correct a finite difference approximation in the vicinity of the interface. MIB-based strategies were originally limited to non-magnetic dielectrics [21, 28] but later generalized to consider a discontinuous electromagnetic field at the interface [22, 27] for 2-D forms of Maxwell's equations. However, the use of complex interfaces and high-order partial derivatives in jump conditions increase the complexity of a MIB strategy as its order increases [26, 28]. It is also worth mentioning that high-order FDTD conforming body approaches have been developed to treat interface conditions for general linear non-magnetic dispersive media in 2-D and 3-D [3]. These approaches could achieve up to fourth-order convergence but they use overlapping grids and therefore a more complex mesh grid.

Another avenue consists of FDTD schemes based on the Correction Function Method (CFM) [18]. Assuming that jumps on the interface can be smoothly extended in its vicinity, the CFM models corrections that are needed to retain the order of a finite difference approximation close to the interface by a system of PDEs based on the original problem. The solution of this system of PDEs is referred as the correction function. Approximations of the correction function are then computed, where it is needed, by minimizing a functional which is a square measure of the error associated with the correction function's system of PDEs. Hence, high-order FDTD schemes can be generated for complex interfaces without significantly increasing the complexity of the proposed numerical strategy. The computational cost increases when compared with the original (i.e. without correction) FD scheme. However, a parallel implementation of the CFM can be easily performed since minimization problems needed for the CFM are independent for a given time step [1]. High-order FD schemes based on the CFM have been originally developed for 2-D Poisson's equation with piecewise constant coefficients [17–19] as well as 3-D Poisson problems with interface jump conditions [20]. In computational electromagnetics, the CFM has been extended to the wave equation [2] and Maxwell's equations [20] with constant coefficients. It is also worth mentioning that high-order CFM-FDTD schemes have been proposed to handle embedded PEC problems [15].

The work presented here generalizes CFM-FDTD approaches to Maxwell's interface problems with discontinuous coefficients. We consider two FDTD schemes, namely the Yee scheme and a fourth-order staggered FDTD scheme, and correct them following the procedure

Fig. 1 Geometry of a domain Ω with an interface Γ



described in [15]. In addition to scattering of a dielectric problems, we also use problems with a manufactured solution for which complete discontinuous electromagnetic fields are considered to demonstrate the robustness and accuracy of the proposed numerical strategy. Finally, we provide numerical evidences that the correction function implicitly satisfies the appropriate high-order jump conditions. Consequently, high-order explicit jump conditions [27, 28] are not required for the presented method.

The paper is organized as follows. In Sect. 2, we introduce a Maxwell’s interface problem. The Correction Function Method is described in Sect. 3. In this same section, we introduce the functional to be minimized based on Maxwell’s equations with interface conditions. The implementation details of the CFM are discussed in Sect. 4. Then, numerical examples are performed in Sect. 5 to verify properties of the proposed CFM-FDTD schemes. Finally, we provide conclusion and outlook in Sect. 6.

2 Definition of the Problem

Assume a domain in space Ω subdivided into two subdomains Ω^+ and Ω^- , and a time interval $I = [0, T]$. The interface Γ between subdomains is independent of time and allows the solutions to be discontinuous. Figure 1 illustrates a typical geometry of a domain Ω .

For a given variable A , we define A^+ and A^- as respectively the solutions in Ω^+ and Ω^- . A jump of A on the interface Γ is denoted as $[[A]] = A^+ - A^-$. Assuming linear media, we consider Maxwell’s equations with interface conditions that are given by

$$\mu(\mathbf{x}) \partial_t \mathbf{H} + \nabla \times \mathbf{E} = 0 \quad \text{in } \Omega \times I, \tag{1a}$$

$$\epsilon(\mathbf{x}) \partial_t \mathbf{E} - \nabla \times \mathbf{H} = 0 \quad \text{in } \Omega \times I, \tag{1b}$$

$$\nabla \cdot (\epsilon(\mathbf{x}) \mathbf{E}) = 0 \quad \text{in } \Omega \times I, \tag{1c}$$

$$\nabla \cdot (\mu(\mathbf{x}) \mathbf{H}) = 0 \quad \text{in } \Omega \times I, \tag{1d}$$

$$\hat{\mathbf{n}} \times [[\mathbf{E}]] = 0 \quad \text{on } \Gamma \times I, \tag{1e}$$

$$\hat{\mathbf{n}} \times [[\mathbf{H}]] = 0 \quad \text{on } \Gamma \times I, \tag{1f}$$

$$\hat{\mathbf{n}} \cdot [[\epsilon(\mathbf{x}) \mathbf{E}]] = 0 \quad \text{on } \Gamma \times I, \tag{1g}$$

$$\hat{\mathbf{n}} \cdot [[\mu(\mathbf{x}) \mathbf{H}]] = 0 \quad \text{on } \Gamma \times I, \tag{1h}$$

$$\mathbf{n} \times \mathbf{H} = \mathbf{g}_1(\mathbf{x}, t) \quad \text{on } \partial\Omega \times I, \tag{1i}$$

$$\mathbf{n} \times \mathbf{E} = \mathbf{g}_2(\mathbf{x}, t) \quad \text{on } \partial\Omega \times I, \tag{1j}$$

$$\mathbf{H}(\mathbf{x}, 0) = \mathbf{H}_0(\mathbf{x}) \quad \text{in } \Omega, \tag{1k}$$

$$\mathbf{E}(\mathbf{x}, 0) = \mathbf{E}_0(\mathbf{x}) \quad \text{in } \Omega, \tag{1l}$$

where \mathbf{H} is the magnetic field, \mathbf{E} is the electric field, $\mu(\mathbf{x}) > 0$ is the magnetic permeability, $\epsilon(\mathbf{x}) > 0$ is the electric permittivity, \mathbf{n} is the unit outward normal to $\partial\Omega$ and $\hat{\mathbf{n}}$ is the unit normal to the interface Γ pointing toward Ω^+ . Interface conditions are given by Eqs. (1e) to (1h) while boundary and initial conditions are given by Eqs. (1i) to (1l). Physical parameters, that is μ and ϵ , can be discontinuous on the interface. Without loss of generality, we assume that electromagnetic fields are at divergence-free in Ω .

3 Correction Function Method

The Correction Function Method (CFM) allows one to find a correction for a given FD approximation involving nodes that belong to different subdomains in order to retain its order. For this purpose, the CFM assumes that solutions in each subdomain can be extended across the interface Γ in a small domain $\Omega_\Gamma \times I$, that is such that $\Omega_\Gamma \subset \Omega$ encloses Γ . A system of PDEs based on the original problem, namely Maxwell’s interface problem (1) in our case, models the extension of each variable around the interface. The solution of this system of PDEs is referred as the correction function. Afterward, we define a functional that is a square measure of the error associated with the correction function’s system of PDEs. Approximations of the correction function are then computed, where it is needed, using a minimization procedure. In practice, the interface is discretized and a local patch $\Omega_\Gamma^h \times I_\Gamma^h \subset \Omega_\Gamma \times I$ is defined for each node of its discretization. Moreover, the size of local patches depends on the considered FD scheme and should diminish as the mesh grid size diminishes.

In the following, we derive the system of PDEs that models the smooth extension of each variable and therefore the correction function. The minimization problem based on an energy functional is also presented. The details on the implementation of the CFM presented here are provided in Sect. 4.

Let us first introduce some notations. The inner product in $L^2(\Omega_\Gamma^h \times I_\Gamma^h)$ is defined by

$$\langle \mathbf{v}, \mathbf{w} \rangle = \int_{I_\Gamma^h} \int_{\Omega_\Gamma^h} \mathbf{v} \cdot \mathbf{w} \, dV \, dt$$

with $\|\mathbf{v}\| = \langle \mathbf{v}, \mathbf{v} \rangle$, and we also use the notation

$$\langle \mathbf{v}, \mathbf{w} \rangle_\Gamma = \int_{I_\Gamma^h} \int_{\Gamma \cap \Omega_\Gamma^h} \mathbf{v} \cdot \mathbf{w} \, dS \, dt$$

with $\|\mathbf{v}\|_\Gamma = \langle \mathbf{v}, \mathbf{v} \rangle_\Gamma$ for legibility. Unlike previous CFM-FDTD schemes, we cannot explicitly model jumps $\mathbf{D}_H = \llbracket \mathbf{H} \rrbracket$ and $\mathbf{D}_E = \llbracket \mathbf{E} \rrbracket$ because of discontinuous coefficients. Hence, we first need to estimate $\mathbf{H}^+, \mathbf{E}^+, \mathbf{H}^-$ and \mathbf{E}^- in the whole patch, and afterward compute an approximation of \mathbf{D}_H and \mathbf{D}_E . The system of PDEs for correction functions is then given by

$$\begin{aligned} \mu^+(\mathbf{x}) \partial_t \mathbf{H}^+ + \nabla \times \mathbf{E}^+ &= 0 \quad \text{in } \Omega_\Gamma^h \times I_\Gamma^h, \\ \epsilon^+(\mathbf{x}) \partial_t \mathbf{E}^+ - \nabla \times \mathbf{H}^+ &= 0 \quad \text{in } \Omega_\Gamma^h \times I_\Gamma^h, \\ \nabla \cdot (\epsilon^+(\mathbf{x}) \mathbf{E}^+) &= 0 \quad \text{in } \Omega_\Gamma^h \times I_\Gamma^h, \\ \nabla \cdot (\mu^+(\mathbf{x}) \mathbf{H}^+) &= 0 \quad \text{in } \Omega_\Gamma^h \times I_\Gamma^h, \\ \mu^-(\mathbf{x}) \partial_t \mathbf{H}^- + \nabla \times \mathbf{E}^- &= 0 \quad \text{in } \Omega_\Gamma^h \times I_\Gamma^h, \end{aligned}$$

$$\begin{aligned}
 \epsilon^-(\mathbf{x}) \partial_t \mathbf{E}^- - \nabla \times \mathbf{H}^- &= 0 \quad \text{in } \Omega_\Gamma^h \times I_\Gamma^h, \\
 \nabla \cdot (\epsilon^-(\mathbf{x}) \mathbf{E}^-) &= 0 \quad \text{in } \Omega_\Gamma^h \times I_\Gamma^h, \\
 \nabla \cdot (\mu^-(\mathbf{x}) \mathbf{H}^-) &= 0 \quad \text{in } \Omega_\Gamma^h \times I_\Gamma^h, \\
 \hat{\mathbf{n}} \times [\mathbf{E}] &= 0 \quad \text{on } \Gamma \cap \Omega_\Gamma^h \times I_\Gamma^h, \\
 \hat{\mathbf{n}} \times [\mathbf{H}] &= 0 \quad \text{on } \Gamma \cap \Omega_\Gamma^h \times I_\Gamma^h, \\
 \hat{\mathbf{n}} \cdot [\epsilon(\mathbf{x}) \mathbf{E}] &= 0 \quad \text{on } \Gamma \cap \Omega_\Gamma^h \times I_\Gamma^h, \\
 \hat{\mathbf{n}} \cdot [\mu(\mathbf{x}) \mathbf{H}] &= 0 \quad \text{on } \Gamma \cap \Omega_\Gamma^h \times I_\Gamma^h,
 \end{aligned} \tag{2}$$

Following the procedure described in [14] to construct a functional that is a square measure of the error associated with system (2) leads to an ill-posed minimization problem. As in CFM-FDTD strategies for embedded perfect electric conductors [15], we can take advantage of FD approximations at previous time steps using fictitious interface conditions to retrieve a well-posed minimization problem. Fictitious interface conditions are given by

$$\begin{aligned}
 \hat{\mathbf{n}}_{1,i}^\circ \times (\mathbf{E}^\circ - \mathbf{E}^{\circ,*}) &= 0 \quad \text{on } \Gamma_{1,i}^\circ \times I_\Gamma^h \quad \text{for } i = 1, \dots, N_1^\circ, \\
 \hat{\mathbf{n}}_{2,i}^\circ \times (\mathbf{H}^\circ - \mathbf{H}^{\circ,*}) &= 0 \quad \text{on } \Gamma_{2,i}^\circ \times I_\Gamma^h \quad \text{for } i = 1, \dots, N_2^\circ, \\
 \hat{\mathbf{n}}_{3,i}^\circ \cdot (\mathbf{E}^\circ - \mathbf{E}^{\circ,*}) &= 0 \quad \text{on } \Gamma_{3,i}^\circ \times I_\Gamma^h \quad \text{for } i = 1, \dots, N_3^\circ, \\
 \hat{\mathbf{n}}_{4,i}^\circ \cdot (\mathbf{H}^\circ - \mathbf{H}^{\circ,*}) &= 0 \quad \text{on } \Gamma_{4,i}^\circ \times I_\Gamma^h \quad \text{for } i = 1, \dots, N_4^\circ,
 \end{aligned} \tag{3}$$

where \circ is either $+$ or $-$ depending in which subdomain the fictitious interface $\Gamma_{k,i}^\circ$ belongs, $\hat{\mathbf{n}}_{k,i}^\circ$ is the normal associated with $\Gamma_{k,i}^\circ$, N_k° is the number of fictitious interfaces, and $\mathbf{H}^{\circ,*}$ and $\mathbf{E}^{\circ,*}$ are approximations of the magnetic field and the electric field that come from a FD scheme.

The quadratic functional to minimize is therefore given by

$$\begin{aligned}
 J(\mathbf{H}^+, \mathbf{E}^+, \mathbf{H}^-, \mathbf{E}^-) &= \frac{\ell_h}{2} \|\mu^+ \partial_t \mathbf{H}^+ + \nabla \times \mathbf{E}^+\| + \frac{\ell_h}{2} \|\epsilon^+ \partial_t \mathbf{E}^+ - \nabla \times \mathbf{H}^+\| \\
 &+ \frac{\ell_h}{2} \|\nabla \cdot (\epsilon^+ \mathbf{E}^+)\| + \frac{\ell_h}{2} \|\nabla \cdot (\mu^+ \mathbf{H}^+)\| + \frac{\ell_h}{2} \|\mu^- \partial_t \mathbf{H}^- + \nabla \times \mathbf{E}^-\| \\
 &+ \frac{\ell_h}{2} \|\epsilon^- \partial_t \mathbf{E}^- - \nabla \times \mathbf{H}^-\| + \frac{\ell_h}{2} \|\nabla \cdot (\epsilon^- \mathbf{E}^-)\| + \frac{\ell_h}{2} \|\nabla \cdot (\mu^- \mathbf{H}^-)\| \\
 &+ \frac{c_p}{2} \|\hat{\mathbf{n}} \times (\mathbf{E}^+ - \mathbf{E}^-)\|_\Gamma + \frac{c_p}{2} \|\hat{\mathbf{n}} \times (\mathbf{H}^+ - \mathbf{H}^-)\|_\Gamma \\
 &+ \frac{c_p}{2} \|\hat{\mathbf{n}} \cdot (\epsilon^+ \mathbf{E}^+ - \epsilon^- \mathbf{E}^-)\|_\Gamma + \frac{c_p}{2} \|\hat{\mathbf{n}} \cdot (\mu^+ \mathbf{H}^+ - \mu^- \mathbf{H}^-)\|_\Gamma \\
 &+ \frac{c_f}{2N_{E^+}} \sum_{i=1}^{N_1^+} \|\hat{\mathbf{n}}_{1,i}^+ \times (\mathbf{E}^+ - \mathbf{E}^{+,*})\|_{\Gamma_{1,i}^+} \\
 &+ \frac{c_f}{2N_{H^+}} \sum_{i=1}^{N_2^+} \|\hat{\mathbf{n}}_{2,i}^+ \times (\mathbf{H}^+ - \mathbf{H}^{+,*})\|_{\Gamma_{2,i}^+} \\
 &+ \frac{c_f}{2N_{E^+}} \sum_{i=1}^{N_3^+} \|\hat{\mathbf{n}}_{3,i}^+ \cdot (\mathbf{E}^+ - \mathbf{E}^{+,*})\|_{\Gamma_{3,i}^+} \\
 &+ \frac{c_f}{2N_{H^+}} \sum_{i=1}^{N_4^+} \|\hat{\mathbf{n}}_{4,i}^+ \cdot (\mathbf{H}^+ - \mathbf{H}^{+,*})\|_{\Gamma_{4,i}^+}
 \end{aligned}$$

$$\begin{aligned}
 &+ \frac{c_f}{2N_{E^-}} \sum_{i=1}^{N_1^-} \|\hat{\mathbf{n}}_{1,i}^- \times (\mathbf{E}^- - \mathbf{E}^{-,*})\|_{\Gamma_{1,i}^-} \\
 &+ \frac{c_f}{2N_{H^-}} \sum_{i=1}^{N_2^-} \|\hat{\mathbf{n}}_{2,i}^- \times (\mathbf{H}^- - \mathbf{H}^{-,*})\|_{\Gamma_{2,i}^-} \\
 &+ \frac{c_f}{2N_{E^-}} \sum_{i=1}^{N_3^-} \|\hat{\mathbf{n}}_{3,i}^- \cdot (\mathbf{E}^- - \mathbf{E}^{-,*})\|_{\Gamma_{3,i}^-} \\
 &+ \frac{c_f}{2N_{H^-}} \sum_{i=1}^{N_4^-} \|\hat{\mathbf{n}}_{4,i}^- \cdot (\mathbf{H}^- - \mathbf{H}^{-,*})\|_{\Gamma_{4,i}^-},
 \end{aligned}$$

where $c_p > 0$ and $c_f > 0$ are penalization coefficients, ℓ_h is the characteristic length in space of the patch, $N_{E^\circ} = N_1^\circ + N_3^\circ$ and $N_{H^\circ} = N_2^\circ + N_4^\circ$. Integrals over the domain are scaled by ℓ_h to guarantee that all terms in the functional J behave in a similar way when the computational grid is refined [14]. The problem statement is then

Find $(\mathbf{H}^+, \mathbf{E}^+, \mathbf{H}^-, \mathbf{E}^-) \in V \times W \times V \times W$ such that

$$(\mathbf{H}^+, \mathbf{E}^+, \mathbf{H}^-, \mathbf{E}^-) \in \underset{\substack{\mathbf{v}^+, \mathbf{v}^- \in V \\ \mathbf{w}^+, \mathbf{w}^- \in W}}{\arg \min} J(\mathbf{v}^+, \mathbf{w}^+, \mathbf{v}^-, \mathbf{w}^-), \tag{4}$$

where $W = V$. Let us recall that we assume divergence-free electromagnetic fields in Ω . We therefore minimize the functional J in a divergence-free space-time polynomial space, namely

$$V = \{ \mathbf{v} \in [P^k(\Omega_\Gamma^h \times I_\Gamma^h)]^3 : \nabla \cdot \mathbf{v} = 0 \},$$

where P^k denotes the space of polynomials of degree k . It is worth mentioning that basis functions of V are based on Legendre polynomials and high-degree divergence-free basis functions proposed in [7].

Remark 1 Using a truncation error analysis, one can show that the order of a CFM-FDTD scheme for Maxwell’s equations (1) is $\min\{n, k\}$ where n is the order of the considered FD scheme and k is the degree of the space-time polynomial space used in minimization problem (4) [15].

Remark 2 The correction function’s system of PDEs on which functional J is based models the extension of each electromagnetic field in the vicinity of the interface while satisfying interface conditions. Hence, by construction and consistency, explicit jump conditions on the interface used for Matched Interface and Boundary based strategies [27, 28] should be implicitly satisfied. Since jump conditions are linear combinations of partial derivatives of correction functions, one should expect a $(k + 1 - q)$ order of convergence for a q -order jump condition, that is a jump condition involving derivatives of order q , when k degree polynomial approximations of correction functions are used. This claim is supported by numerical evidences presented in Sect. 5.1.

Remark 3 It is recalled that fictitious interface conditions are used to retrieve a well-posed minimization problem. Regarding the value of c_f , the priority should be given to interface conditions and therefore $c_p > c_f > 0$. Moreover, c_f should also diminish as the mesh grid

size diminishes to enforce again interface conditions. It is worth mentioning that fictitious interfaces impact the stability of a FDTD scheme when the CFM is applied. As mentioned in [15], the stability analysis of a CFM-FDTD scheme that uses fictitious interface conditions (3) is not trivial. Despite the lack of a rigorous proof, a sufficient small value of c_f seems to avoid any stability issues that would stem from the CFM. However, one should be aware that a too small value of c_f could lead to poorly conditioned matrices coming from minimization problem (4). We also assume that the stability condition of a CFM-FDTD scheme should be close to the one associated with the original (i.e. without correction) FDTD scheme.

4 Implementation of the CFM

In this section, we provide some technical details on the implementation of the CFM. We first begin by a description of the computation of fictitious interface conditions and local patches. Afterward, the implementation of the minimization procedure is discussed.

4.1 Computation of Fictitious Interface Conditions

Fictitious interface conditions (3), which are needed to retrieve a well-posed minimization problem, use fictitious interfaces $\Gamma_{k,i}$ on which previous computed FD approximations, that is \mathbf{H}^* and \mathbf{E}^* , are available. In the following, we provide the main steps of the computation of fictitious interface conditions.

We first generate the fictitious interfaces in such a way that they are aligned with the mesh grid and that their endpoints coincide with mesh grid nodes. Hence, the normal $\hat{\mathbf{n}}_{k,i}$ associated with these fictitious interfaces is an element of the standard basis in \mathbb{R}^3 . This also provides us the interval of integration in space associated with each fictitious interface and facilitates the computation of space-time interpolants that are needed to compute the associated integrals in minimization problem (4). Figure 2 illustrates an example of fictitious interfaces in subdomain Ω^+ that could be generated in a 2-D local patch when a staggered grid is used. Regarding the interval of integration in time, this strongly depends on the chosen time-stepping method and can be defined beforehand. As an example, we refer the reader to Sections 4 and 5 of [15] where the CFM is applied on the Yee scheme and a fourth-order staggered FDTD scheme. Once fictitious interfaces are generated, we can identify the mesh grid nodes that coincide with them and therefore their associated FD approximations. This allows us to directly construct space-time Lagrange polynomials using FD approximations of previous time steps and use them to compute space-time integrals involving fictitious interface conditions in the minimization problem.

Remark 4 The initialization of CFM-FDTD schemes can be difficult because of time integrals involving \mathbf{H}^* and \mathbf{E}^* . An initialization strategy has been proposed in [15] for the Yee scheme and a fourth-order FDTD scheme based on a multistep method. It is worth mentioning that this initialization strategy is also used in this work. Another approach, which is specific to some applications, consists to assume that electromagnetic fields close to the interface remain unchanged for $t \leq t_0$.

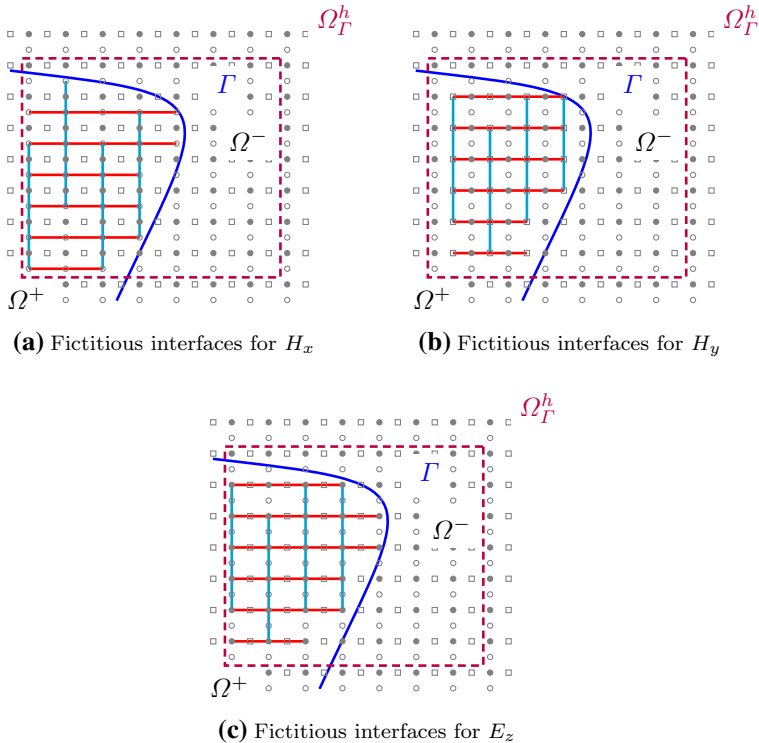


Fig. 2 An example of a local patch Ω_Γ^h with fictitious interfaces in subdomain Ω^+ . The x -component and the y -component of the magnetic field are respectively represented by \circ and \square while the z -component of the electric field is represented by \bullet . Fictitious interfaces associated with $\mathbf{n}_1 = (1, 0)$ and $\mathbf{n}_2 = (0, 1)$ are respectively represented by --- and --- . Reprinted by permission from Springer Nature Customer Service Centre GmbH: Springer Nature, Journal of Scientific Computing, FDTD Schemes for Maxwell’s equations with Embedded Perfect Electric Conductors Based on the Correction Function Method, Y.-M. Law and J.-C. Nave, Copyright 2021 (Color figure online)

4.2 Computation of Local Patches

The accuracy of approximations of correction functions depends strongly on local patches used in the minimization procedure. Indeed, the interface Γ must be well-represented within the patch since the information used to estimate correction functions, that is interface conditions (1e) to (1h), stem from it. To achieve this, we directly discretize the interface as it is done for immersed boundary methods [13, 15, 23]. Let us assume a 2-D domain and a parametrization of the interface Γ with respect to $s \in [s_a, s_b]$. The number of local patches is given by

$$N_s \approx \frac{L_\Gamma}{\alpha h} + 1$$

where α is a positive constant, h is the mesh grid size and L_Γ is the estimated arc length of the interface. Thus, the coordinates of the centre point of local patches are

$$\mathbf{x}_{c,i} = (x(s_i), y(s_i))$$

for $i = 0, \dots, N_s - 1$, where $s_i = s_a + i \Delta s$ and $\Delta s = \frac{s_b - s_a}{N_s - 1}$.

Once these centre points are determined, the domain $\Omega_{\Gamma}^h \times I_{\Gamma}^h$ of local patches is computed. The size in space of local patches ℓ_h should depend on the mesh grid size, that is $\ell_h = \beta \max\{\Delta x, \Delta y, \Delta z\}$, where β is a positive constant. The choice of β depends on the considered FD scheme and must allow the construction of enough fictitious interfaces within the local patch. To ease the implementation, local patches are taken aligned with the mesh grid and square in space. The time domain I_{Γ}^h depends on the chosen time-stepping method and we refer to [15] for some examples involving staggered grids in time. Afterward, each node to be corrected is associated with its closest $x_{c,i}$ and therefore with a local patch. Finally, it is worth noting that the node to be corrected must also be included in its local patch.

4.3 Minimization Problems

The minimization procedure is of foremost importance for the CFM since this method heavily relies on it to compute estimations of correction functions that are used to retain the order of a given FD scheme. Moreover, minimization problems could increase dramatically the computational cost of a CFM-FDTD scheme if the minimization procedure is not properly implemented. In the following, we describe the minimization procedure and provide some details on its implementation.

Computing Gateaux derivatives of functional J and using a necessary condition to obtain a minimum, we obtain a linear system of the form

$$M \mathbf{c} = c_f \mathbf{b}_f + c_p \mathbf{b}_{\Gamma} \quad (5)$$

where \mathbf{c} is a vector containing the coefficients of polynomial approximations of correction functions, and \mathbf{b}_{Γ} and \mathbf{b}_f are associated with terms involving respectively interface conditions and fictitious interface conditions. It is worth mentioning that $\mathbf{b}_{\Gamma} = 0$ for Maxwell's interface problem (1). The computation of the vector \mathbf{b}_f involves the space-time integration of \mathbf{H}^* and \mathbf{E}^* , which come from previous computed FD approximations and are therefore known.

Since the time domain I_{Γ}^h of local patches translates as the time increases, we only need to compute one matrix M for each space domain Ω_{Γ}^h . Let us assume a single interface, we therefore have a total of N_s different matrices M to compute. One should compute these matrices, their scaling and LU factorizations beforehand. Otherwise, the computational time of a CFM-FDTD scheme will be much greater than the one of its original FDTD scheme. Once this is done, we therefore need to compute the right-hand side of system (5), perform a forward substitution and a back substitution to obtain \mathbf{c} , and estimate correction functions at the appropriate nodes for each local patch and at each time step. It is worth mentioning that the computational cost of a single minimization problem does not increase as the mesh grid size diminishes. However, the number of local patches N_s , which scales as $\frac{1}{h}$, increases as h diminishes. In general, the computational cost of the CFM scales as N^{d-1} for a uniform mesh grid of N^d nodes, where d is the dimension and N is the number of nodes in each dimension [17]. Hence, the computational cost of the CFM becomes less significant for large problems. Although it is not used in this work, it is worth mentioning that a parallel implementation of the CFM can be easily performed since minimization problems needed for the CFM are independent at each time step [1]. This could therefore further reduce the cost of the CFM.

Remark 5 For schemes that use staggered grids in time, one should be careful when computing minimization problems. Let us consider the Yee scheme as an example. For this scheme, we need two sets of minimization problems. A set for the update of the magnetic field at $t_{n+1/2}$ and another one for the update of the electric field at t_{n+1} .

5 Numerical Examples

In this section, we perform convergence analysis and long-time simulations in 2-D to verify the proposed numerical strategy. We consider the transverse magnetic (TM_z) mode. Hence, for a domain $\Omega \subset \mathbb{R}^2$, Maxwell’s equations are simplified to

$$\begin{aligned}
 \mu(x, y) \partial_t H_x + \partial_y E_z &= 0 \quad \text{in } \Omega \times I, \\
 \mu(x, y) \partial_t H_y - \partial_x E_z &= 0 \quad \text{in } \Omega \times I, \\
 \epsilon(x, y) \partial_t E_z - \partial_x H_y + \partial_y H_x &= 0 \quad \text{in } \Omega \times I, \\
 \partial_x(\mu(x, y) H_x) + \partial_y(\mu(x, y) H_y) &= 0 \quad \text{in } \Omega \times I,
 \end{aligned}
 \tag{6}$$

with the associated interface, boundary and initial conditions. In this 2-D simplification of Maxwell’s equations, electromagnetic fields are continuous across the interface between the vacuum and a non-magnetic dielectric material. However, for a magnetic dielectric material, the electric field is still continuous across the interface while the magnetic field could be discontinuous.

We consider two different FDTD schemes, namely the Yee scheme and a fourth-order FDTD scheme, which is referred as the FD-4th scheme in this work. The latter FDTD scheme also uses staggered grids in both space and time. More specifically, space derivatives are estimated with the fourth-order centered FD approximation for staggered grids while time derivatives are estimated using a fourth-order staggered free-parameter multistep method [11]. Considering $\partial_t \mathbf{H} = \mathbf{f}_H(\mathbf{E})$ and $\partial_t \mathbf{E} = \mathbf{f}_E(\mathbf{H})$, the considered fourth-order time-stepping method is given by

$$\begin{aligned}
 \mathbf{H}^{n+1/2} &= -\alpha_3 \mathbf{H}^{n-1/2} - \alpha_2 \mathbf{H}^{n-3/2} - \alpha_1 \mathbf{H}^{n-5/2} - \alpha_0 \mathbf{H}^{n-7/2} + \\
 &\quad \Delta t (\beta_3 \mathbf{f}_H(\mathbf{E}^n) + \beta_2 \mathbf{f}_H(\mathbf{E}^{n-1}) + \beta_1 \mathbf{f}_H(\mathbf{E}^{n-2})), \\
 \mathbf{E}^{n+1} &= -\alpha_3 \mathbf{E}^n - \alpha_2 \mathbf{E}^{n-1} - \alpha_1 \mathbf{E}^{n-2} - \alpha_0 \mathbf{E}^{n-3} + \\
 &\quad \Delta t (\beta_3 \mathbf{f}_E(\mathbf{H}^{n+1/2}) + \beta_2 \mathbf{f}_E(\mathbf{H}^{n-1/2}) + \beta_1 \mathbf{f}_E(\mathbf{H}^{n-3/2})),
 \end{aligned}$$

where $\beta_1 = t, \beta_2 = s, \beta_3 = \frac{1}{22} s + \frac{12}{11}$,

$$\begin{aligned}
 \alpha_0 &= -\frac{1}{22} - \frac{1}{528} s + \frac{1}{24} t, \\
 \alpha_1 &= \frac{5}{22} + \frac{9}{176} s - \frac{9}{8} t, \\
 \alpha_2 &= -\frac{9}{22} - \frac{201}{176} s + \frac{9}{8} t, \\
 \alpha_3 &= -\frac{17}{22} + \frac{577}{528} s - \frac{1}{24} t
 \end{aligned}$$

with $s = -1$ and $t = 1.045$.

The associated CFM-FDTD schemes are then the CFM-Yee scheme and the CFM-4th scheme. We refer to [15] for more details on the application of the CFM on these two FDTD schemes. Since a staggered grid in time is used, the error of $\mathbf{U} = [H_x, H_y, E_z]^T$ at a given time t is computed using approximations and exact solutions of the magnetic field and the electric field at respectively $t - \frac{\Delta t}{2}$ and t .

5.1 Scattering of a Dielectric Cylinder Problems

Let us consider a dielectric cylinder in free-space exposed to a TM_z excitation wave. The interface is a circle of radius $r_0 = 0.6$ centered at $(0, 0)$. The exact solution in cylindrical coordinates is given by the real part of

$$\begin{aligned}
 H_\theta(r, \theta, t) &= \begin{cases} -\frac{ik^-}{\omega\mu^-} \sum_{n=-\infty}^{\infty} C_n^{\text{tot}} J'_n(k^- r) e^{i(n\theta + \omega t)}, & \text{if } r \leq r_0, \\ -\frac{ik^+}{\omega\mu^+} \sum_{n=-\infty}^{\infty} (i^{-n} J'_n(k^+ r) + C_n^{\text{scat}} H_n^{(2)'}(k^+ r)) e^{i(n\theta + \omega t)}, & \text{if } r > r_0, \end{cases} \\
 H_r(r, \theta, t) &= \begin{cases} -\frac{1}{\omega\mu^- r} \sum_{n=-\infty}^{\infty} n C_n^{\text{tot}} J_n(k^- r) e^{i(n\theta + \omega t)}, & \text{if } r \leq r_0, \\ -\frac{1}{\omega\mu^+ r} \sum_{n=-\infty}^{\infty} n (i^{-n} J_n(k^+ r) + C_n^{\text{scat}} H_n^{(2)}(k^+ r)) e^{i(n\theta + \omega t)}, & \text{if } r > r_0, \end{cases} \\
 E_z(r, \theta, t) &= \begin{cases} \sum_{n=-\infty}^{\infty} C_n^{\text{tot}} J_n(k^- r) e^{i(n\theta + \omega t)}, & \text{if } r \leq r_0, \\ \sum_{n=-\infty}^{\infty} (i^{-n} J_n(k^+ r) + C_n^{\text{scat}} H_n^{(2)}(k^+ r)) e^{i(n\theta + \omega t)}, & \text{if } r > r_0, \end{cases}
 \end{aligned}$$

with

$$\begin{aligned}
 C_n^{\text{tot}} &= i^{-n} \frac{\frac{k^+}{\mu^+} (J'_n(k^+ r_0) H_n^{(2)}(k^+ r_0) - H_n^{(2)'}(k^+ r_0) J_n(k^+ r_0))}{\frac{k^-}{\mu^-} J'_n(k^- r_0) H_n^{(2)}(k^+ r_0) - \frac{k^+}{\mu^+} H_n^{(2)'}(k^+ r_0) J_n(k^- r_0)}, \\
 C_n^{\text{scat}} &= i^{-n} \frac{\frac{k^+}{\mu^+} J'_n(k^+ r_0) J_n(k^- r_0) - \frac{k^-}{\mu^-} J'_n(k^- r_0) J_n(k^+ r_0)}{\frac{k^-}{\mu^-} J'_n(k^- r_0) H_n^{(2)}(k^+ r_0) - \frac{k^+}{\mu^+} H_n^{(2)'}(k^+ r_0) J_n(k^- r_0)},
 \end{aligned}$$

where i is the imaginary number, $k^\circ = \omega \sqrt{\mu^\circ \epsilon^\circ}$, $\omega = 2\pi$, J_n is the n -order Bessel function of first kind and $H_n^{(2)}$ is the n -order Hankel function of second kind [5, 24].

Since this work focuses on the treatment of interface conditions, we therefore enforce the exact solution on the boundary $\partial\Omega$ of the domain $\Omega = [-1, 1] \times [-1, 1]$ instead of using absorbing boundary conditions. For the Yee and CFM-Yee schemes, we impose Dirichlet boundary conditions on all $\partial\Omega$. As for the FD-4th and CFM-4th schemes, we directly enforce the exact solution on nodes that are close to the boundary $\partial\Omega$ and on which the fourth-order centered FD scheme cannot be used.

The time interval is $I = [0, 1]$. The mesh grid size is $h = \Delta x = \Delta y$ with $h \in \{\frac{1}{20}, \frac{1}{28}, \frac{1}{40}, \frac{1}{52}, \frac{1}{72}, \frac{1}{96}, \frac{1}{132}, \frac{1}{180}, \frac{1}{244}, \frac{1}{336}\}$ and the time-step size is $\Delta t = \frac{h}{2}$. For both CFM-FDTD schemes, we choose $\alpha = 6$ and $\ell_h = 7h$ to construct local patches, and we use at least a second degree interpolating polynomial in space to construct \mathbf{H}^* and \mathbf{E}^* that are needed for fictitious interface conditions (3). We set $c_f = \Delta t$ and $c_f = \frac{\Delta t}{4}$ for respectively the CFM-Yee and CFM-4th schemes while $c_p = 1$ for both schemes. Second and third degree polynomial approximations of correction functions are chosen for respectively the CFM-Yee and CFM-4th schemes.

Let us first consider $\mu^+ = \mu^- = 1$, $\epsilon^+ = 1$ and $\epsilon^- = 2.25$. This corresponds to a non-magnetic dielectric material, and therefore H_x , H_y and E_z are continuous across the interface. Figure 7a illustrates the convergence plot of $\mathbf{U} = [H_x, H_y, E_z]^T$ for both CFM-FDTD schemes and their original FDTD schemes, that is without correction. We observe a rough second-order convergence in L^2 -norm for the Yee scheme while a clear second-order

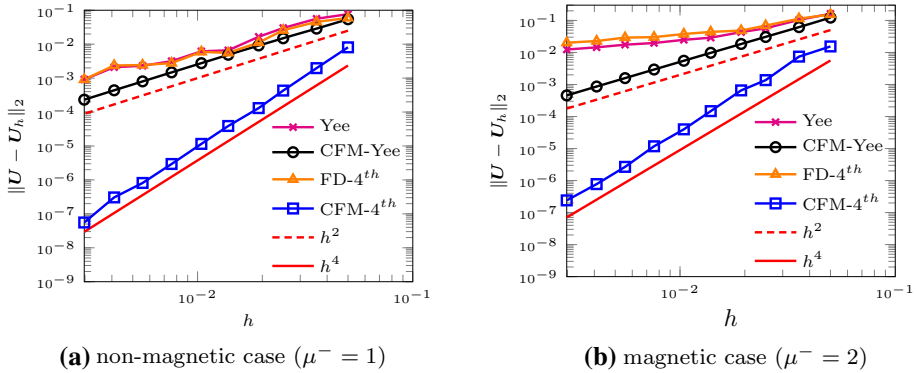


Fig. 3 Convergence plots for scattering of a dielectric cylinder problems with $\mu^+ = 1, \epsilon^+ = 1$ and $\epsilon^- = 2.25$ using the proposed CFM-FDTD schemes and their associated original FDTD schemes. It is recalled that $U = [H_x, H_y, E_z]^T$

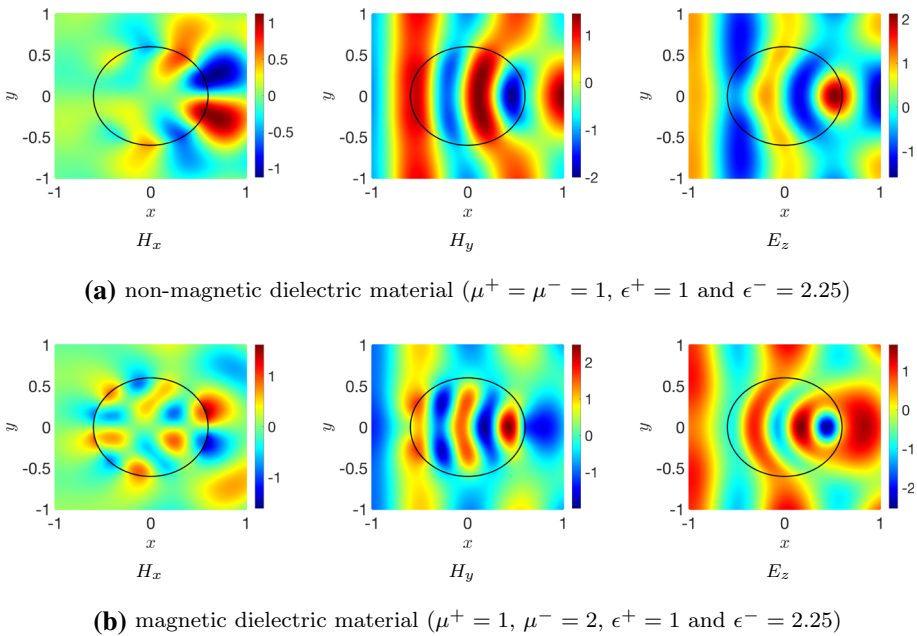


Fig. 4 The components H_x, H_y and E_z with $h = \frac{1}{244}$ for scattering of a dielectric cylinder problems using the CFM-4th scheme. The approximate electric field and magnetic field are shown respectively at $t = 1$ and $t - \frac{\Delta t}{2}$. The interface is represented by the black line (Color figure online)

convergence is obtained for the CFM-Yee scheme. A rough second-order convergence is also observed for the FD-4th scheme, which is suboptimal. This could be explained by the use of a staircased approximation of the interface, which leads to a first-order approximation of the geometry of the problem, and by the fact that interface conditions are not explicitly enforced [8]. For the CFM-4th scheme, a fourth-order convergence is retrieved, which is better than expected (see Remark 1). Numerical solutions computed with the CFM-4th scheme at $t = 1$ are illustrated in Fig. 4a.

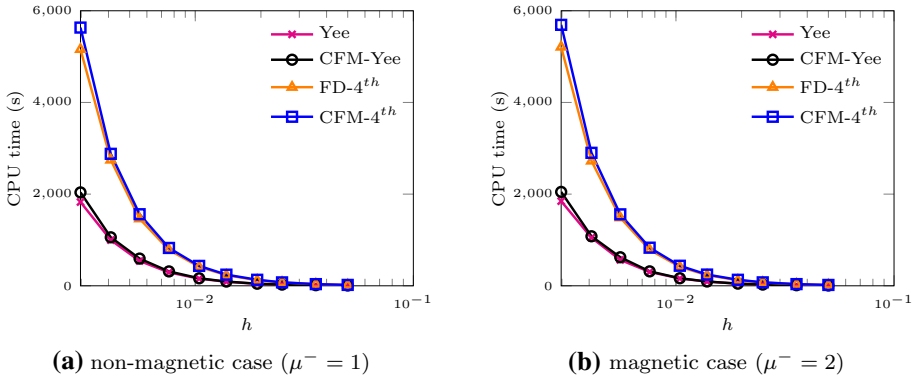


Fig. 5 The CPU time of time iterations in function of the mesh grid size for scattering of a dielectric cylinder problems with $\mu^+ = 1$, $\epsilon^+ = 1$ and $\epsilon^- = 2.25$ using the proposed CFM-FDTD schemes and their associated original FDTD schemes

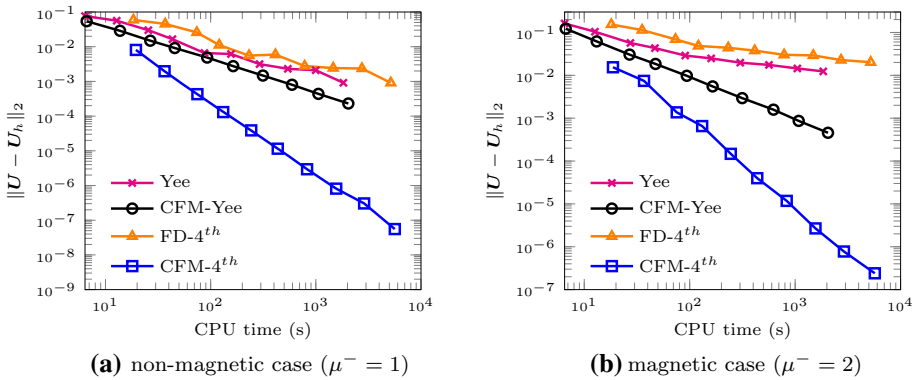


Fig. 6 The error in L^2 -norm in function of the CPU time of time iterations for scattering of a dielectric cylinder problems with $\mu^+ = 1$, $\epsilon^+ = 1$ and $\epsilon^- = 2.25$ using the proposed CFM-FDTD schemes and their associated original FDTD schemes. It is recalled that $U = [H_x, H_y, E_z]^T$

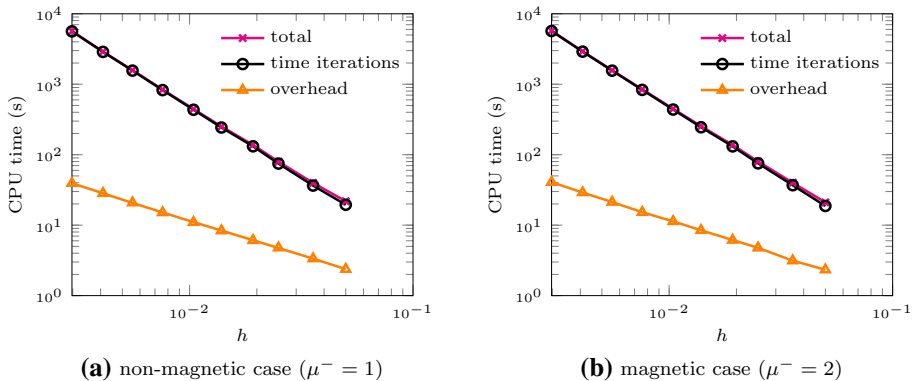


Fig. 7 The detailed CPU time in function of the mesh grid size for scattering of a dielectric cylinder problems with $\mu^+ = 1$, $\epsilon^+ = 1$ and $\epsilon^- = 2.25$ using the CFM-4th scheme

Let us now consider a magnetic dielectric material. We choose $\mu^+ = 1$, $\mu^- = 2$, $\epsilon^+ = 1$ and $\epsilon^- = 2.25$. In this case, the components of the magnetic field are discontinuous while the z -component of the electric field is still continuous across the interface. Figure 7b illustrates the convergence plot of electromagnetic fields for all considered FDTD schemes. Both the Yee and FD-4th schemes have a convergence order lower than one, which is expected since the magnetic field is discontinuous across the interface. A second and fourth order convergence in L^2 -norm are observed for respectively the CFM-Yee and CFM-4th schemes. Thus, the CFM allows one to retain the order of a given FDTD scheme while enforcing interface conditions. These results are in agreement with the theory. Figure 4b illustrates the approximation of H_x , H_y and E_z at $t = 1$ using the CFM-4th scheme.

5.1.1 Computational Time of the CFM

Let us now assess the extra computational time associated with the CFM by computing CPU times of all FDTD schemes in both magnetic and non-magnetic cases. The computational time is computed using the BenchmarkTools package [6] available in the Julia programming language [4]. Figures 5 and 6 show respectively the CPU time of time iterations in function of the mesh grid size and the error in L^2 -norm in function of the CPU time of time iterations for all FDTD schemes and both cases. As shown in Fig. 5, a CFM-FDTD scheme takes more computational time than its original FDTD scheme for a given mesh grid size. As expected, we also observe that the computational time of the CFM increases with the degree of the polynomial space of correction functions' approximations or when the number of local patches increases, that is when the mesh grid size diminishes. However, since the CFM retains the order of a given FDTD scheme, FDTD schemes based on the CFM take much less time than their original FDTD schemes to reach a given error, as illustrated in Fig. 6. This is particularly noticeable for the magnetic case and for the CFM-4th scheme. Figure 7 shows the total CPU time, and those for the overhead treatment needed for the CFM, that is the computation of local patches and the construction of the matrices M (see Sect. 4.3), and time iterations in function of the mesh grid size when the CFM-4th scheme is used. As the mesh grid size diminishes, the cost of the overhead part of the CFM becomes negligible when compared with the CPU time of time iterations.

5.1.2 Verification of the Accuracy of Correction Functions

In this subsection, we assess the accuracy of the estimated correction functions coming from minimization problem (4) using high-order explicit jump conditions [27, 28]. Matched Interface and Boundary (MIB) based strategies use these conditions to construct high-order FDTD schemes. As mentioned in Remark 2, the correction function's system of PDEs implicitly considers jump conditions coming from Maxwell's equations (1). To provide numerical evidences of this claim, we compute the error on these jump conditions on all local patches using

$$\left(\int_{\Gamma \cap \Omega_t^q} \llbracket u(\mathbf{x}, T) \rrbracket^2 dS \right)^{1/2},$$

where $\llbracket u(\mathbf{x}, T) \rrbracket$ is a given jump condition evaluated with approximate solutions of problem (4) at the final time $T = 1$. Afterward, the maximum error value on all local patches for a given order of jump conditions is taken and is denoted by E_q for the q -order jump condition.

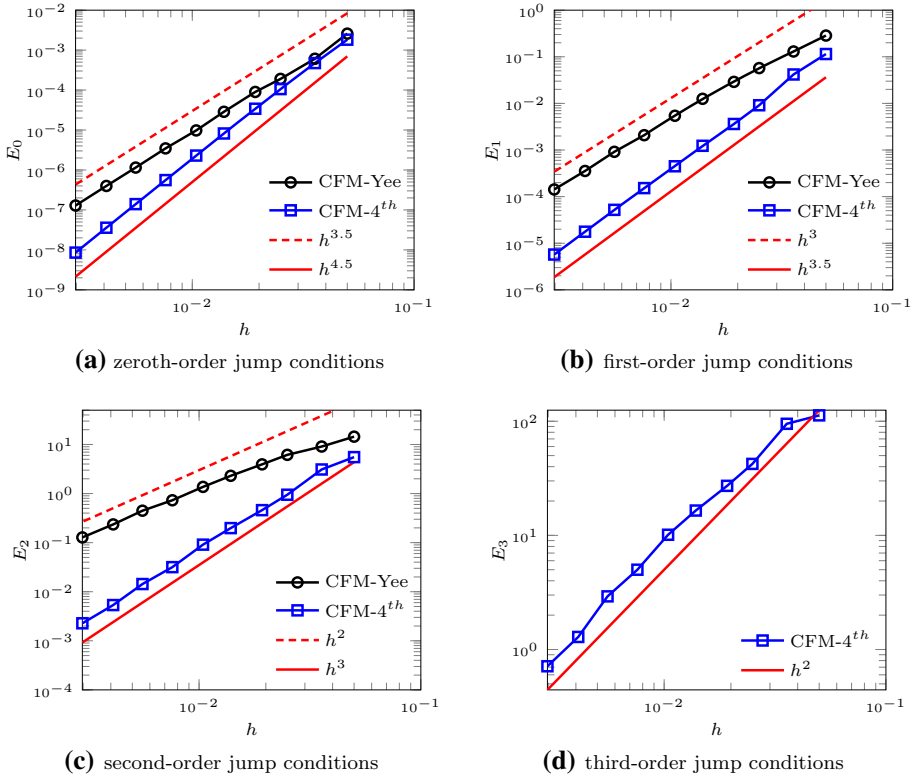


Fig. 8 Convergence plots of jump conditions for a scattering of a non-magnetic dielectric cylinder problem ($\mu^+ = \mu^- = 1$) using the proposed CFM-FDTD schemes. The red lines represent the observed convergence reference curves (Color figure online)

For a non-magnetic dielectric material, high-order jump conditions can be derived by using the continuity of time derivatives of electromagnetic fields on the interface [28] and are given by:

$$\begin{aligned}
 \text{zeroth-order} & \begin{cases} \llbracket H_x \rrbracket = 0, \\ \llbracket H_y \rrbracket = 0, \\ \llbracket E_z \rrbracket = 0, \end{cases} & \text{first-order} & \begin{cases} \llbracket \partial_y E_z \rrbracket = 0, \\ \llbracket \partial_x E_z \rrbracket = 0, \\ \llbracket \frac{1}{\epsilon} (\partial_x H_y - \partial_y H_x) \rrbracket = 0, \end{cases} \\
 \text{second-order} & \begin{cases} \llbracket \frac{1}{\epsilon} (\partial_x^2 E_z - \partial_y^2 E_z) \rrbracket = 0, \\ \llbracket \frac{1}{\epsilon} (\partial_y^2 H_x - \partial_{xy}^2 H_y) \rrbracket = 0, \\ \llbracket \frac{1}{\epsilon} (\partial_x^2 H_y - \partial_{xy}^2 H_x) \rrbracket = 0, \end{cases} \\
 \text{third-order} & \begin{cases} \llbracket \frac{1}{\epsilon} (\partial_{xxy}^3 E_z + \partial_y^3 E_z) \rrbracket = 0, \\ \llbracket \frac{1}{\epsilon} (\partial_x^3 E_z + \partial_{xyy}^3 E_z) \rrbracket = 0, \\ \llbracket \frac{1}{\epsilon^2} (\partial_x^3 H_y + \partial_{xyy}^3 H_y - \partial_y^3 H_x - \partial_{xxy}^3 H_x) \rrbracket = 0. \end{cases}
 \end{aligned}$$

Figure 8 illustrates convergence plots of those jump conditions at $T = 1$ for both CFM-FDTD schemes. We observe that the convergence order for all jump conditions is better than expected (see Remark 2).

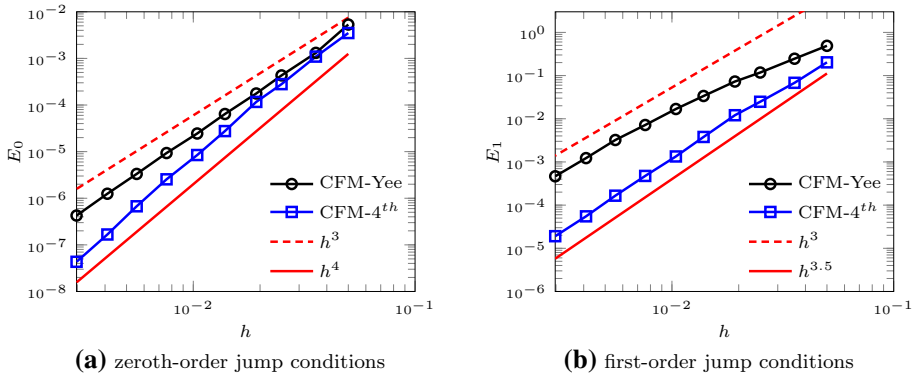


Fig. 9 Convergence plots of jump conditions for a scattering of a magnetic dielectric cylinder problem with $\mu^+ = 1$ and $\mu^- = 2$ using the proposed CFM-FDTD schemes. The red lines represent the observed convergence reference curves (Color figure online)

Let us now consider a magnetic dielectric material. Considering a point $\mathbf{p} = (x_p, y_p)$ on the interface Γ , one can define a local coordinate system based on the normal \mathbf{n} and the tangent $\boldsymbol{\tau}$ to the interface at \mathbf{p} , and derive explicit jump conditions coming from Maxwell’s equations (1) [27]. In this local coordinate system, zeroth and first order jump conditions are given by

$$\begin{aligned}
 \text{zeroth-order} & \begin{cases} \llbracket H_\tau \rrbracket = 0, \\ \llbracket \mu H_n \rrbracket = 0, \\ \llbracket E_z \rrbracket = 0, \end{cases} \\
 \text{first-order} & \begin{cases} \llbracket \partial_\tau E_z \rrbracket = 0, \\ \llbracket \frac{1}{\mu} \partial_n E_z \rrbracket = 0, \\ \llbracket \partial_n(\mu H_n) + \partial_\tau(\mu H_\tau) \rrbracket = 0, \\ \llbracket \partial_n(\mu H_\tau) - \partial_\tau(\mu H_n) - \partial_t(\mu \epsilon E_z) \rrbracket = 0. \end{cases} \tag{7}
 \end{aligned}$$

Convergence plots of zeroth and first order jump conditions at $T = 1$ are shown in Fig. 9 for both CFM-FDTD schemes. A third-order convergence is observed for zeroth and first order jump conditions when the CFM-Yee scheme is used. As for the CFM-4th scheme, a fourth-order convergence is obtained for zeroth-order jump conditions while a three and a half order convergence is observed for first-order jump conditions. According to numerical results, approximations of correction functions coming from minimization problem (4) are consistent with high-order explicit jump conditions coming from Maxwell’s equations (1) and therefore are appropriate to correct FD approximations in the vicinity of the interface.

5.2 Problems with a Manufactured Solution

To our knowledge, there is no analytic solution for Maxwell’s interface problems with an arbitrary geometry of the interface. In order to verify the proposed numerical strategy, general interface conditions, given by

$$\hat{\mathbf{n}} \times \llbracket \mathbf{E} \rrbracket = \mathbf{a}(\mathbf{x}, t) \quad \text{on } \Gamma \times I, \tag{8a}$$

$$\hat{\mathbf{n}} \times \llbracket \mathbf{H} \rrbracket = \mathbf{b}(\mathbf{x}, t) \quad \text{on } \Gamma \times I, \tag{8b}$$

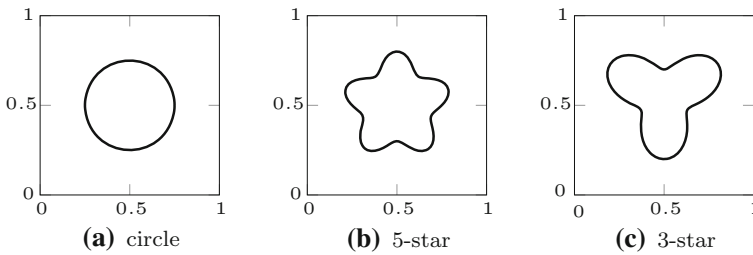


Fig. 10 Different geometries of the interface

$$\hat{n} \cdot \llbracket \epsilon(\mathbf{x}) \mathbf{E} \rrbracket = c(\mathbf{x}, t) \quad \text{on } \Gamma \times I, \tag{8c}$$

$$\hat{n} \cdot \llbracket \mu(\mathbf{x}) \mathbf{H} \rrbracket = d(\mathbf{x}, t) \quad \text{on } \Gamma \times I, \tag{8d}$$

are considered. Hence, both tangential and normal components of electromagnetic fields can be discontinuous on the interface. Moreover, electromagnetic fields are at divergence-free in each subdomain, but not necessarily in the whole domain because of interface conditions (8c) and (8d). Source terms in each subdomain are given by $f_1^+(\mathbf{x}, t)$ and $f_1^-(\mathbf{x}, t)$ for Faraday’s law (1a), and by $f_2^+(\mathbf{x}, t)$ and $f_2^-(\mathbf{x}, t)$ for Ampère-Maxwell’s law (1b). It is worth mentioning that these source terms and interface conditions are not substantiated by physics. Nevertheless, they can be used to construct manufactured solutions that are needed to verify the proposed numerical strategy for arbitrary complex interfaces.

The domain is $\Omega = [0, 1] \times [0, 1]$ and the time interval is $I = [0, 1]$. The physical parameters are given by $\mu^+ = 2, \epsilon^+ = 1, \mu^- = \sin(5\pi xy) + 2$ and $\epsilon^- = 2e^{xy}$. The magnetic permeability and electric permittivity have been chosen in such a way that electromagnetic fields are at divergence-free in each subdomain. The manufactured solutions are:

$$\begin{aligned} H_x^+ &= 0.5 \sin(2\pi x) \sin(2\pi y) \sin(2\pi t), \\ H_y^+ &= 0.5 \cos(2\pi x) \cos(2\pi y) \sin(2\pi t), \\ E_z^+ &= \sin(2\pi x) \cos(2\pi y) \cos(2\pi t) \end{aligned}$$

in Ω^+ , and

$$\begin{aligned} H_x^- &= -x e^{-xy} \sin(2\pi t), \\ H_y^- &= y e^{-xy} \sin(2\pi t), \\ E_z^- &= \sin(2\pi xy) \cos(2\pi t) \end{aligned}$$

in Ω^- . The associated source terms are $f_1^+ = 0, f_2^+ = 0,$

$$\begin{aligned} f_{1,x}^- &= 2\pi x (\cos(2\pi xy) - (\sin(5\pi xy) + 2) e^{-xy}) \cos(2\pi t), \\ f_{1,y}^- &= 2\pi y ((\sin(5\pi xy) + 2) e^{-xy} - \cos(2\pi xy)) \cos(2\pi t), \\ f_2^- &= ((x^2 + y^2) e^{-xy} - 4\pi e^{xy} \sin(2\pi xy)) \sin(2\pi t). \end{aligned}$$

We consider geometries of the interface that are illustrated in Fig. 10. Periodic boundary conditions are imposed on all $\partial\Omega$ for both CFM-FDTD schemes. The mesh grid size is $h = \Delta x = \Delta y$ and the time-step size is $\Delta t = \frac{h}{2}$ with $h \in \{\frac{1}{20}, \frac{1}{28}, \frac{1}{40}, \frac{1}{52}, \frac{1}{72}, \frac{1}{96}, \frac{1}{132}, \frac{1}{180}, \frac{1}{244}, \frac{1}{336}, \frac{1}{460}\}$. All other parameters are the same as in Sect. 5.1. Figure 11 shows convergence plots of $\mathbf{U} = [H_x, H_y, E_z]^T$ for all geometries of the

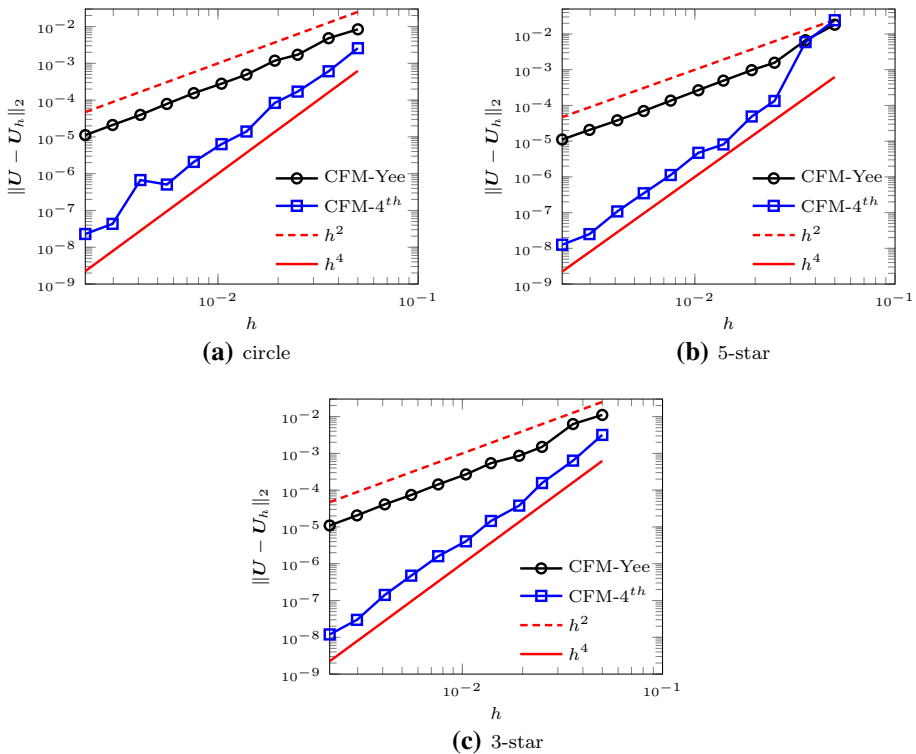


Fig. 11 Convergence plots for problems with a manufactured solution using the proposed CFM-FDTD schemes and various geometries of the interface. It is recalled that $U = [H_x, H_y, E_z]^T$

interface. We observe a second-order convergence in L^2 -norm for the CFM-Yee scheme. As for the CFM-4th scheme, a global fourth-order convergence is observed using the L^2 -norm for all interfaces. These results are in agreement with the theory. Figure 12 illustrates the approximate solutions for different geometries of the interface. One can observe that there is no spurious oscillation in the vicinity of the interface.

5.3 Stability Investigation: Long-Time Simulations

As mentioned in Remark 3, a rigorous stability analysis of CFM-FDTD schemes is out of reach for the moment. In this short subsection, we therefore investigate the stability of CFM-FDTD schemes using long-time simulations. We consider a problem with a manufactured solution and a 3-star interface presented in Sect. 5.2. We use the CFM-Yee and CFM-4th schemes. We consider a larger time interval, given by $I = [0, 300]$, and different values of the penalization coefficient c_f associated with fictitious interface conditions. All other parameters remain the same as previously described.

Figure 13(a) illustrates the evolution of the error in L^2 -norm of electromagnetic fields using the CFM-Yee scheme, $h = \frac{1}{80}$ and different values of the penalization coefficient c_f . The CFM-Yee scheme seems to be stable for a sufficient low value of c_f , that is Δt^2 in this case. We also observe that the error increases as c_f diminishes. Figure 13(b) shows the evolution of the error for various mesh grid sizes using $c_f = \Delta t^2$. For all mesh grids,

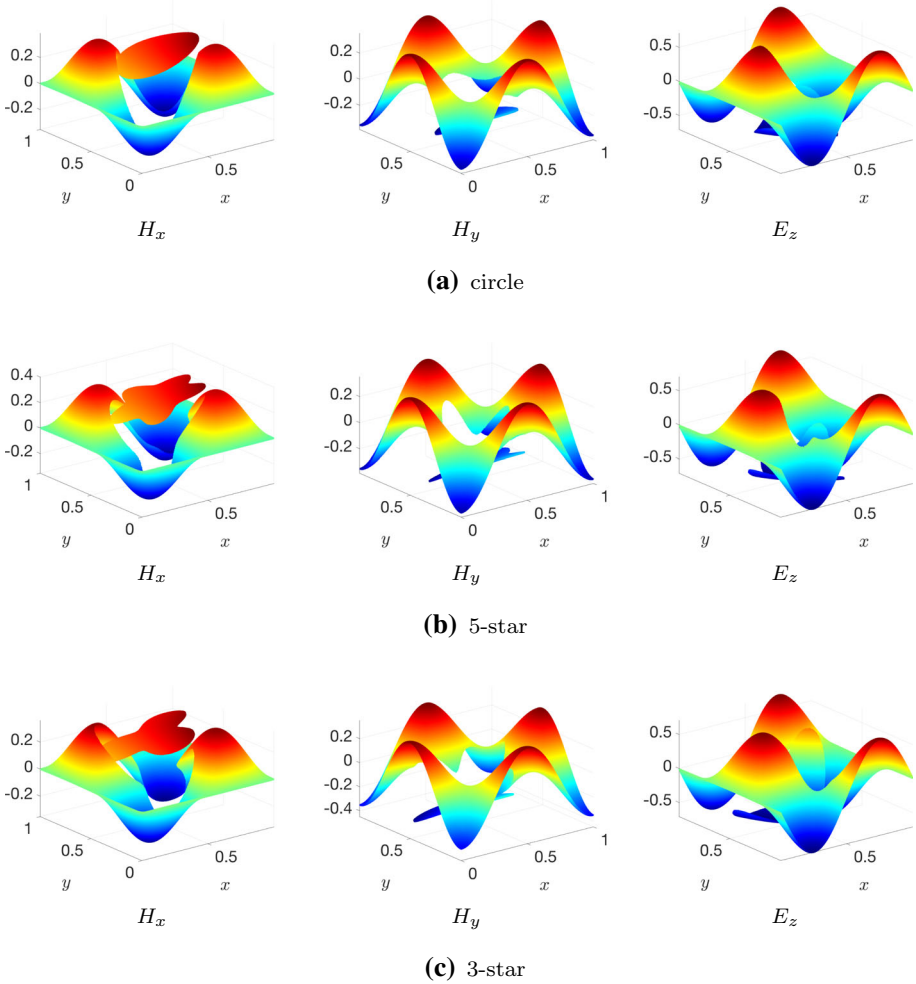


Fig. 12 The components H_x , H_y and E_z with $h = \frac{1}{336}$ for problems with a manufactured solution using the CFM-Yee scheme and various geometries of the interface. The approximate electric field and magnetic field are shown respectively at $t = 0.625$ and $t - \frac{\Delta t}{2}$

numerical results suggest that the CFM-Yee scheme is stable for the considered value of c_f . Figure 14(a) illustrates the evolution of the error in L^2 -norm using the CFM-4th scheme, $h = \frac{1}{80}$ and various values of c_f . In contrast to the CFM-Yee scheme, an error growth appears after $t = 65$ even for the smallest considered penalization coefficient, that is $c_f = \Delta t^3$. Figure 14(b) shows the evolution of the error for various mesh grid sizes using $c_f = \Delta t^3$. As the mesh grid size diminishes, the error growth seems to occur at a larger time.

As mentioned in Remark 3, a sufficient small value of c_f should avoid any stability issues that would stem from the CFM. To provide numerical evidences of this claim, we perform long-time simulations using the Yee and FD-4th schemes with the same settings as their associated CFM-FDTD schemes. Figure 15 illustrates the evolution of the error in L^2 -norm for various mesh grid sizes using both schemes. Although these schemes provide

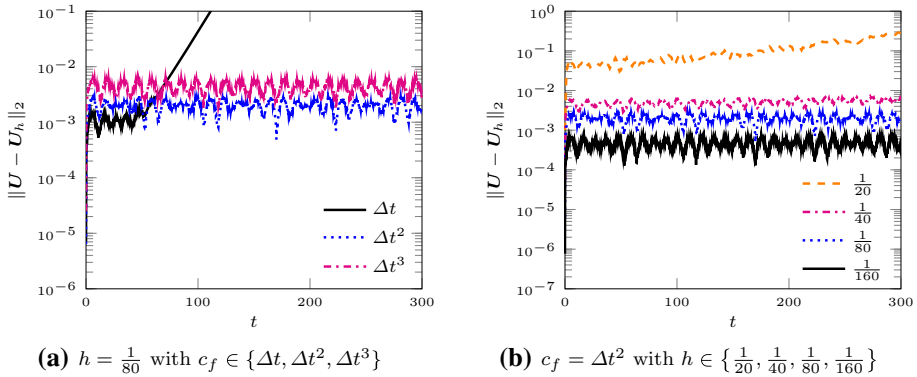


Fig. 13 Evolution of the error in L^2 -norm of $U = [H_x, H_y, E_z]^T$ for a problem with a manufactured solution using a 3-star interface, the CFM-Yee scheme, and different mesh grid sizes and values of c_f

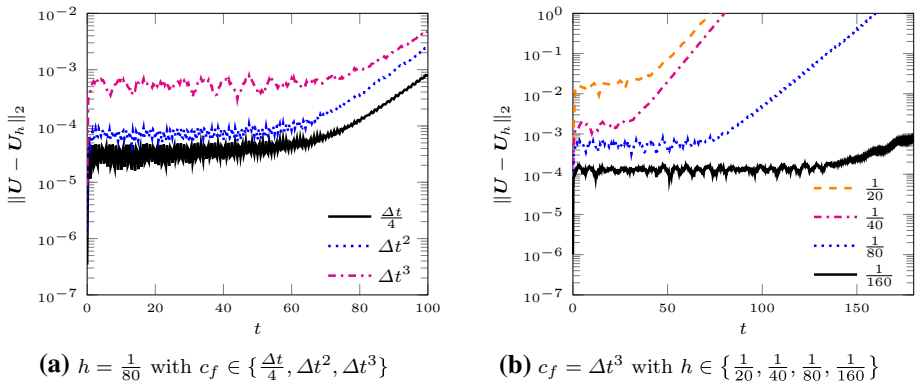


Fig. 14 Evolution of the error in L^2 -norm of $U = [H_x, H_y, E_z]^T$ for a problem with a manufactured solution using a 3-star interface, the CFM-4th scheme, and different mesh grid sizes and values of c_f

non-convergent approximations, we can observe that the Yee scheme is stable while there are error growths when we use the FD-4th scheme. It worth noting that these error growths occur around the same time as when we consider its associated CFM-FDTD scheme. Thus, a CFM-FDTD scheme inherits the stability properties of the associated original FDTD scheme for a sufficient small c_f while retaining its order.

5.4 Scattering of a Magnetic Dielectric Problems

Let us consider scattering problems involving various geometries, which are illustrated in Fig. 10, of a magnetic dielectric material in free-space. We assume the subdomain Ω^- to be a magnetic dielectric material and therefore this subdomain is enclosed by the interface Γ . The domain is $\Omega = [-1, 1.5] \times [-0.75, 1.75]$ and the time interval is $I = [0, 1.5]$. We set $\mu^+ = 1, \mu^- = 2, \epsilon^+ = 1$ and $\epsilon^- = 2.5$. The components of the magnetic field could therefore be discontinuous across the interface Γ . Periodic boundary conditions are

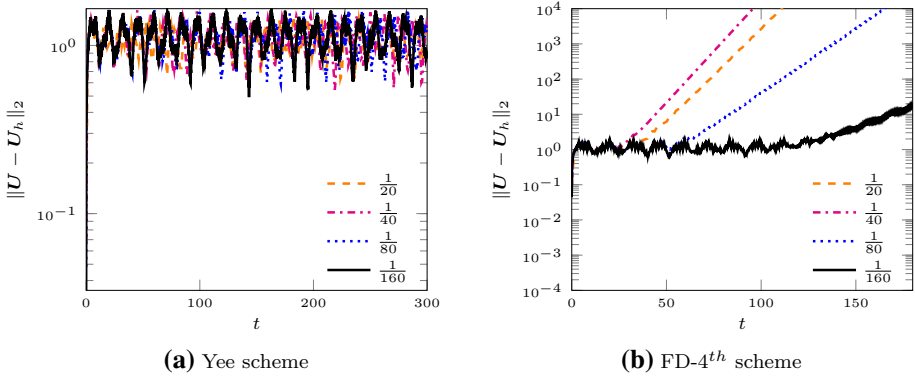


Fig. 15 Evolution of the error in L^2 -norm of $U = [H_x, H_y, E_z]^T$ for a problem with a manufactured solution using a 3-star interface with either the Yee scheme or the FD-4th scheme. We consider different mesh grid sizes, that is $h \in \{ \frac{1}{20}, \frac{1}{40}, \frac{1}{80}, \frac{1}{160} \}$

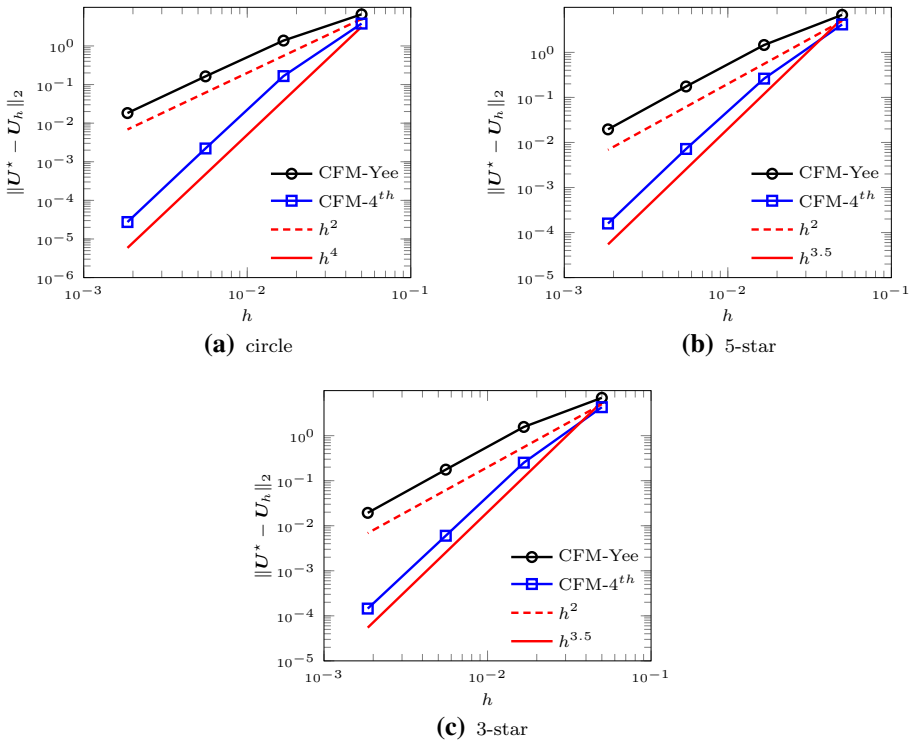


Fig. 16 Convergence plots for scattering of a magnetic dielectric problems using the proposed CFM-FDTD schemes and various geometries of the interface. It is recalled that $U = [H_x, H_y, E_z]^T$

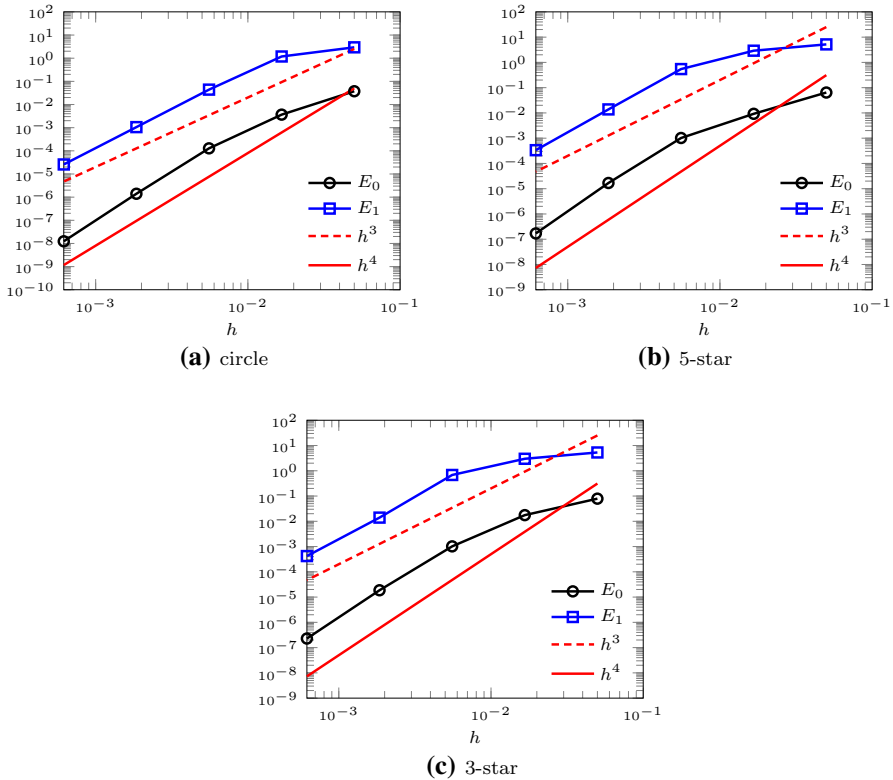


Fig. 17 Convergence plots of the zeroth and first order jump conditions for scattering of a magnetic dielectric problems using the CFM-4th scheme and various geometries of the interface. The red lines represent the observed convergence reference curves (Color figure online)

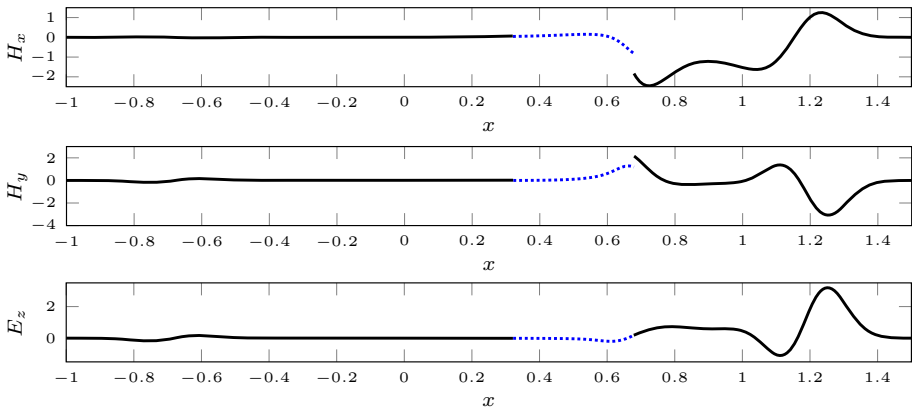


Fig. 18 The electromagnetic fields along the x -axis at $y \approx 0.3253$ for H_x , and $y = 0.3250$ for H_y and E_z for the scattering of a circular magnetic dielectric problem using the CFM-4th scheme and $h = \frac{1}{1620}$. The computed electric field and magnetic field are shown respectively at $t = 1.5$ and $t = \frac{\Delta t}{2}$. The approximate solutions in Ω^+ and Ω^- correspond to respectively the black line and dotted blue line (Color figure online)

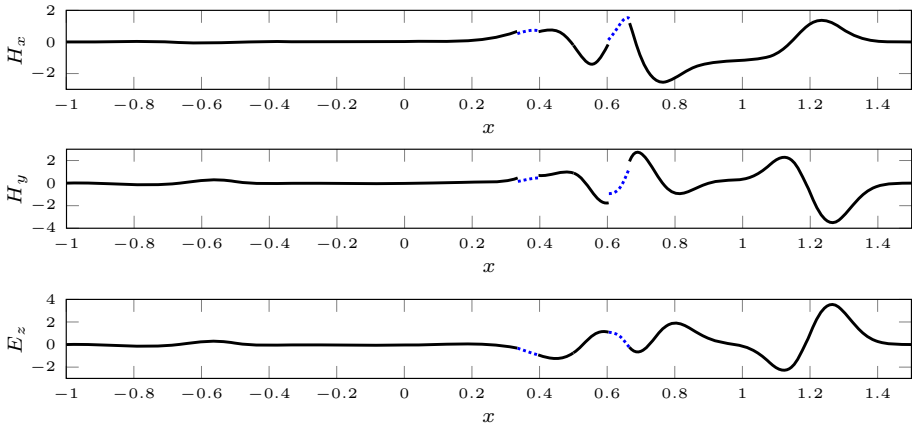


Fig. 19 The electromagnetic fields along the x -axis at $y \approx 0.2512$ for H_x , and $y \approx 0.2509$ for H_y and E_z for the scattering of a 5-star magnetic dielectric problem using the CFM-4th scheme and $h = \frac{1}{1620}$. The computed electric field and magnetic field are shown respectively at $t = 1.5$ and $t - \frac{\Delta t}{2}$. The approximate solutions in Ω^+ and Ω^- correspond to respectively the black line and dotted blue line (Color figure online)

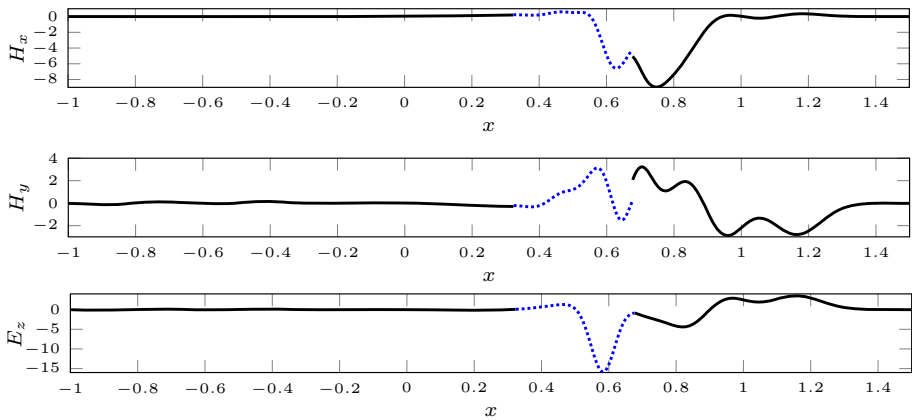


Fig. 20 The electromagnetic fields along the x -axis at $y \approx 0.5056$ for H_x , and $y \approx 0.5052$ for H_y and E_z for the scattering of a 3-star magnetic dielectric problem using the CFM-4th scheme and $h = \frac{1}{1620}$. The computed electric field and magnetic field are shown respectively at $t = 1.5$ and $t - \frac{\Delta t}{2}$. The approximate solutions in Ω^+ and Ω^- correspond to respectively the black line and dotted blue line (Color figure online)

considered on all $\partial\Omega$. The incoming pulsed electromagnetic wave is described by

$$\begin{aligned}
 H_{x_p}(\mathbf{x}, t) &= 0, \\
 H_{y_p}(\mathbf{x}, t) &= -\frac{2}{\sigma^2} (x - \gamma - t) e^{-\left(\frac{x-\gamma-t}{\sigma}\right)^2}, \\
 E_{z_p}(\mathbf{x}, t) &= \frac{2}{\sigma^2} (x - \gamma - t) e^{-\left(\frac{x-\gamma-t}{\sigma}\right)^2},
 \end{aligned} \tag{9}$$

where $\gamma = -0.3$ and $\sigma = 0.1$. The electromagnetic fields given in (9) are also used to initialize the considered time-stepping methods. As mentioned before, to our knowledge, there

is no analytic solution for arbitrary geometries of the interface. Hence, we use approximate solutions coming from a very fine mesh grid as the reference solution, denoted U^* , to estimate errors.

The mesh grid size is $h = \Delta x = \Delta y$ with $h \in \left\{ \frac{1}{20}, \frac{1}{60}, \frac{1}{180}, \frac{1}{540} \right\}$ and the time-step size is $\Delta t = \frac{h}{2}$. We use $h = \frac{1}{1620}$ for the reference solution and therefore all nodes used in coarser mesh grids are also part of the finest mesh grid. All other parameters are the same as in Sect. 5.1. Figure 16 illustrates convergence plots for both CFM-FDTD schemes and all interfaces. As expected, a second-order convergence in L^2 -norm is obtained for the CFM-Yee scheme. As for the CFM-4th scheme, we observe a fourth-order convergence for the circular dielectric material, while a three and a half order convergence is observed for the 3-star and 5-star dielectric materials. Convergence plots for the zeroth (E_0) and first (E_1) order jump conditions, given in (7), for the CFM-4th scheme are illustrated in Fig. 17. It is worth mentioning that errors on jump conditions can also be computed on the reference solution. As expected, we obtain a fourth and third order convergence for respectively the zeroth and first order jump conditions. This suggests that finer mesh grids are required to clearly obtain a fourth-order convergence for U using the 3-star and 5-star interfaces. The results are in agreement with the theory. Figures 18, 19 and 20 show approximate electromagnetic fields along the x -axis for the considered interfaces. The discontinuities within approximate solutions are captured without spurious oscillation.

6 Conclusions

In this work, we presented high-order FDTD schemes based on the Correction Function Method to handle Maxwell's interface problems. The system of PDEs needed for the CFM was derived using Maxwell's equations with interface conditions. The minimization problem based on a functional that is a square measure of the error associated with the correction function's system of PDEs was also presented. Numerical examples showed that numerical solutions coming from CFM-FDTD schemes were captured without spurious oscillation while exhibiting high-order convergence. It has also been shown that FDTD schemes based on the CFM take much less computational time than their original FDTD schemes to reach a given error. Moreover, the accuracy of correction functions has been verified using high-order explicit jump conditions. This showed that high-order jump conditions are implicitly enforced in the functional to minimize and therefore need not be provided explicitly. Scattering of a dielectric problems and problems with a manufactured solution have shown that the proposed numerical strategy can handle various geometries of the interface without significantly increasing the complexity of the method. Since fictitious interface conditions impact the stability of a CFM-FDTD scheme, long-time simulations have been performed. Numerical evidences support our claim that a CFM-FDTD scheme inherits the stability properties of the associated original FDTD scheme, that is without correction, for a sufficient small c_f while retaining its order. Future work will focus on the theoretical aspect of the CFM as well as an extension of this strategy to 3-D problems.

Acknowledgements The authors are grateful to Alexis Montoisson of Polytechnique Montréal for his help on the Julia programming language. The authors also thank Dr. Jessica Lin and Dr. Gantumur Tsogtgerel of McGill University for their support.

Funding The research of JCN was partially supported by the NSERC Discovery Program.

Declarations

Conflict of interest The authors have no relevant financial or non-financial interests to disclose.

Availability of data and material All data generated or analyzed during this study are included in this article.

Code availability The custom code used for this work is not yet publicly available.

References

1. Abraham, D.S., Giannacopoulos, D.D.: A parallel implementation of the correction function method for Poisson's equation with immersed surface charges. *IEEE Trans. Magn.* **53**(6) (2017)
2. Abraham, D.S., Marques, A.N., Nave, J.C.: A correction function method for the wave equation with interface jump conditions. *J. Comput. Phys.* **353**, 281–299 (2018)
3. Banks, J.W., Buckner, B.B., Henshaw, W.D., Jenkinson, M.J., Kildishev, A.V., Kovačič, G., Prokopeva, L.J., Schwendeman, D.W.: A high-order accurate scheme for Maxwell's equations with a Generalized Dispersive Material (GDM) model and material interfaces. *J. Comput. Phys.* **412**, 109424 (2020)
4. Bezanson, J., Edelman, A., Karpinski, S., Shah, V.B.: Julia: a fresh approach to numerical computing. *SIAM Rev.* **59**, 65–98 (2017)
5. Cai, W., Deng, S.: An upwinding embedded boundary method for Maxwell's equations in media with material interfaces: 2D case. *J. Comput. Phys.* **190**, 159–183 (2003)
6. Chen, J., Jarrett, R.: Robust benchmarking in noisy environments. In: *HPEC'16 Proceedings of the Twentieth IEEE High Performance Extreme Computing Conference*. IEEE (2016)
7. Cockburn, B., Li, F., Shu, C.W.: Locally divergence-free discontinuous Galerkin methods for the Maxwell equations. *J. Comput. Phys.* **194**(2), 588–610 (2004)
8. Ditkowski, A., Dridi, K., Hesthaven, J.S.: Convergent cartesian grid methods for Maxwell equations in complex geometries. *J. Comput. Phys.* **170**, 39–80 (2001)
9. Dridi, K., Hesthaven, J.S., Ditkowski, A.: Staircase-free finite-difference time-domain formulation for general materials in complex geometries. *IEEE Trans. Antennas Propag.* **49**(5), 749–756 (2001)
10. Fedkiw, R.P., Aslam, T., Merriman, B., Osher, S.: A non-oscillatory Eulerian approach to interfaces in multimaterial flows (the ghost fluid method). *J. Comput. Phys.* **152**, 457–492 (1999)
11. Ghrist, M., Fornberg, B., Driscoll, T.A.: Staggered time integrators for wave equations. *SIAM J. Numer. Anal.* **38**, 718–741 (2000)
12. Hesthaven, J.S.: High-order accurate methods in time-domain computational electromagnetics: a review. *Adv. Imag. Electron Phys.* **127**, 59–123 (2003)
13. Kallemov, B., Bhalla, A.P.S., Griffith, B.E., Donev, A.: An immersed boundary method for rigid bodies. *Commun. Appl. Math. Comput. Sci.* **11**, 79–141 (2016)
14. Law, Y.M., Marques, A.N., Nave, J.C.: Treatment of complex interfaces for Maxwell's equations with continuous coefficients using the correction function method. *J. Sci. Comput.* **82**(3), 56 (2020)
15. Law, Y.M., Nave, J.C.: FDTD schemes for Maxwell's equations with embedded perfect electric conductors based on the correction function method. *J. Sci. Comput.* **88**(3), 72 (2021)
16. LeVeque, R.J., Li, Z.: The immersed interface method for Elliptic equations with discontinuous coefficients and singular sources. *SIAM J. Num. Anal.* **31**(4), 1019–1044 (1994)
17. Marques, A.N.: A correction function method to solve incompressible fluid flows to high accuracy with immersed geometries. Ph.D. thesis, Massachusetts Institute of Technology (2012)
18. Marques, A.N., Nave, J.C., Rosales, R.R.: A correction function method for Poisson problems with interface jump conditions. *J. Comput. Phys.* **230**, 7567–7597 (2011)
19. Marques, A.N., Nave, J.C., Rosales, R.R.: High order solution of Poisson problems with piecewise constant coefficients and interface jumps. *J. Comput. Phys.* **335**, 497–515 (2017)
20. Marques, A.N., Nave, J.C., Rosales, R.R.: Imposing jump conditions on nonconforming interfaces for the correction function method: a least squares approach. *J. Comput. Phys.* **397**, 108869 (2019)
21. Nguyen, D.D., Zhao, S.: A new high order dispersive FDTD method for Drude material with complex interfaces. *J. Comput. Appl. Math.* **289**, 1–14 (2015)
22. Nguyen, D.D., Zhao, S.: A second order dispersive FDTD algorithm for transverse electric Maxwell's equations with complex interfaces. *Comput. Math. Appl.* **71**, 1010–1035 (2016)
23. Stein, D.B., Guy, R.D., Thomases, B.: Immersed boundary smooth extension: a high-order method for solving PDE on arbitrary smooth domains using Fourier spectral methods. *J. Comput. Phys.* **304**, 252–274 (2016)

24. Taflove, A.: *Computational Electrodynamics?: The Finite Difference Time-domain Method*. Artech House, Norwood (1995)
25. Yee, K.S.: Numerical solution of initial boundary value problems involving Maxwell's equations in isotropic media. *IEEE Trans. Antennas Propag.* **14**(3), 302–307 (1966)
26. Yu, S., Zhou, Y., Wei, G.W.: Matched interface and boundary (MIB) method for elliptic problems with sharp-edged interfaces. *J. Comput. Phys.* **224**, 729–756 (2007)
27. Zhang, Y., Nguyen, D.D., Du, K., Xu, J., Zhao, S.: Time-domain numerical solutions of Maxwell interface problems with discontinuous electromagnetic waves. *Adv. Appl. Math. Mech.* **8**, 353–385 (2016)
28. Zhao, S., Wei, G.W.: High-order FDTD methods via derivative matching for Maxwell's equations with material interfaces. *J. Comput. Phys.* **200**, 60–103 (2004)

Publisher's Note Springer Nature remains neutral with regard to jurisdictional claims in published maps and institutional affiliations.